Energies **2014**, *7*, 7348-7367; doi:10.3390/en7117348

OPEN ACCESS

energies

ISSN 1996-1073

www.mdpi.com/journal/energies

Article

Design Optimization of Heat Wheels for Energy Recovery in HVAC Systems

Stefano De Antonellis [1,*], Manuel Intini [1], Cesare Maria Joppolo [1] and Calogero Leone [2]

[1] Department of Energy, Politecnico di Milano, Via Lambruschini 4, Milano 20156, Italy; E-Mails: manuel.intini@polimi.it (M.I.); cesare.joppolo@polimi.it (C.M.J.)

[2] Recuperator S.p.A., Via Valfurva 13, Rescaldina (MI) 20027, Italy; E-Mail: leone@recuperator.eu

* Author to whom correspondence should be addressed; E-Mail: stefano.deantonellis@polimi.it; Tel.: +39-02-2399-3823; Fax: +39-02-2399-3863.

External Editor: Chi-Ming Lai

Received: 31 July 2014; in revised form: 13 September 2014 / Accepted: 4 November 2014 / Published: 14 November 2014

Abstract: Air to air heat exchangers play a crucial role in mechanical ventilation equipment, due to the potential primary energy savings both in case of refurbishment of existing buildings or in case of new ones. In particular, interest in heat wheels is increasing due to their low pressure drop and high effectiveness. In this paper a detailed optimization of design parameters of heat wheels is performed in order to maximize sensible effectiveness and to minimize pressure drop. The analysis is carried out through a one dimensional lumped parameters heat wheel model, which solves heat and mass transfer equations, and through appropriate correlations to estimate pressure drop. Simulation results have been compared with experimental data of a heat wheel tested in specific facilities, and good agreement is attained. The device optimization is performed through the variation of main design parameters, such as heat wheel length, channel base, height and thickness and for different operating conditions, namely the air face velocity and the revolution speed. It is shown that the best configurations are achieved with small channel thickness and, depending on the required sensible effectiveness, with appropriate values of wheel length and channel base and height.

Keywords: heat wheel optimization; heat wheel effectiveness; simulation; experimental data; heat exchanger design

1. Introduction

It is well known that buildings are responsible for around 40% of primary energy consumption in developed countries and for 20%–40% in developing countries [1]. In case of refurbishment of existing buildings or in new ones, the introduction of a heat exchanger between exhaust and fresh air streams play a crucial role due to relevant achievable energy savings [2–8]. In particular, interest in heat wheels is increasing due to their low pressure drop and high effectiveness compared to conventional plate heat exchangers [9].

As shown in Figure 1, a heat wheel consists of a cylindrical rotating device which is obtained rolling up corrugated sheets of a metallic material (such as aluminium) in order to get a large number of parallel channels with a typical sinusoidal cross sectional geometry. Two air streams pass through the cross sectional area of the device: The supply one, which is the fresh air stream, and the exhaust one, which is the return air flow from the building. A purge sector between exhaust and supply air streams is often used in order to reduce contamination of the fresh air flow. Heat is transferred from one air stream to the wheel matrix and then from the matrix to the other stream. If one of the two flows reaches the dew point, water is also transferred between the two streams.

Figure 1. Scheme of heat wheel and channel control volume.

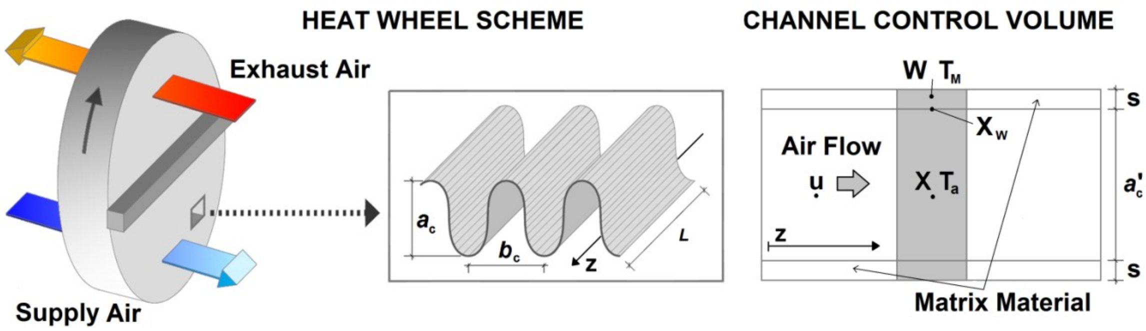

Many research activities have been carried out to improve heat wheels' performance. There are several works dealing with rotary heat exchangers modeling [10–13] or focusing on the development of practical effectiveness and pressure drop correlations to be used in energy system simulations [14–17]. Further works analyse experimental performance of heat wheels, enthalpy wheels and desiccant wheels [18–20], evaluating the optimal working conditions. A few papers deal with the design of rotary heat exchangers based on non-dimensional parameters [21] or the *ε-NTU* (Number of Transfer Units) method [22]. The first study is particularly complex and results are shown for a limited number of cases, while the second one is based on a simplified approach. Research studies have been focused also on the optimization of heat transfer rate in channel crossed by a laminar flow [23].

Anyway in the previous works no clear guidelines about geometry and matrix material specifications of rotary heat exchangers are provided. The aim of this work is to provide a detailed analysis and optimization of heat wheel design, maximizing sensible effectiveness and minimizing pressure drop. In particular the effects of channel geometry, wheel length and revolution speed on component performance are evaluated.

The analysis of the rotary heat exchanger has been performed through a lumped parameter model based on heat and mass transfer equations and on appropriate correlations to evaluate pressure drop. The model has been previously validated through the comparison with the performance of a rotary device tested in the lab facilities, showing good agreements in all the conditions.

2. Mathematical Model

2.1. Heat Wheel Description and Model Assumptions

The rotating wheel, which is characterized by a diameter D and a length L, is divided into two sections: the first for supply air and the second for exhaust air in a counter current flow arrangement. The wheel rotates at constant speed N and each channel is periodically exposed to the two streams. In this model the purge section is not considered.

As shown in Figure 1, the geometry of the channel cross section is assumed sinusoidal in the upper part and flat in the remaining one. Duct height and base are respectively referred to as a_c and b_c. The physical model and the numerical analysis are based on the following assumptions:

- Temperature and velocity profiles in the channels are fully developed.
- Channels are equal and uniformly distributed throughout the wheel.
- Temperature, humidity ratio and velocity of each inlet flow are uniform at the inlet face of the wheel.
- Heat and mass transfer between adjacent channels is negligible.
- Heat and mass transfer from the wheel to the surroundings is negligible.
- Axial heat conduction and water vapour diffusion in the air stream are negligible.
- Temperature gradient through the channel thickness is negligible.
- Density and velocity variation of air along the channel are negligible.
- Specific heat and thermal conductivity of dry air, water vapour and liquid water are assumed constant.
- Air leakages between the two streams are negligible.

2.2. Governing Equations

The following equations are applied to an infinitesimal element of the channel: Conservation of water and energy in the solid side (matrix material and condensed water), conservation of water and energy in the wet air stream.

Conservation of water in the air stream:

$$\frac{\partial X}{\partial t} = -\frac{\partial X}{\partial z}u - \frac{P\,h_m}{\rho_{da}A_c}(X - X_w) \tag{1}$$

where X is the humidity ratio of the air stream, X_W is the humidity ratio of air on the channel wall, P the perimeter and A_c the cross sectional area of the channel and h_m the mass transfer coefficient.

Conservation of water on the channel surface:

$$\frac{\partial W}{\partial t} = \frac{h_m (X - X_w)\, P}{f_M} \tag{2}$$

where W is the amount of condensed water on the channel surface and f_M is the metallic material mass per unit of length in the channel.

Energy balance in the system made up of the matrix material and the condensed water:

$$(f_M cp_M + f_M cp_w W)\frac{\partial T_M}{\partial t} = (cp_v T_a - cp_w T_M + \lambda) h_m (X - X_w)\, P + h_T (T_a - T_M) P + A_M k_M \frac{\partial^2 T_M}{\partial z^2} \tag{3}$$

where T_a and T_M are respectively the air and channel material temperature, λ is the vaporization latent heat of water, cp_w and cp_M are respectively the specific heat of the liquid water and of the channel material, h_T is the heat transfer coefficient, k_M and A_M are respectively the thermal conductivity and the cross sectional area of the matrix thickness.

Energy balance in the air stream:

$$\frac{\partial T_a}{\partial t} = -u\frac{\partial T_a}{\partial z} - \frac{h_T\, (T_a - T_M)\, P}{A_c \rho_{da}\, cp_{wa}} - \frac{h_m\, (X - X_W) P cp_v T_a}{A_c \rho_{da}\, cp_{wa}} \tag{4}$$

where cp_{wa} is the specific heat of wet air defined as $cp_{wa} = cp_{da} + X \cdot cp_v$.

Further equations are necessary to solve the system. The humidity ratio on the surface of the channel structure can be expressed in the form reported in the following. If water condensation occurs on the surface ($W > 0$) or the surface temperature is below the dew point of the air stream ($T_M < T_{dew}$):

$$X_W = X_W\left(T_M; \varphi = 100\%\right) \tag{5a}$$

In all other conditions:

$$X_W = X \tag{5b}$$

The relation between relative and absolute humidity is:

$$X = 0.622\frac{\varphi}{\frac{p_{tot}}{p_{sat}} - \varphi} \tag{6}$$

where p_{tot} is the atmospheric pressure, assumed constant and equal to 101,325 Pa, and p_{sat} is the steam saturation pressure, calculated through the following equation:

$$p_{sat} = e^{\left(23.196 - \frac{381644}{T_a + 273.15 - 46.13}\right)} \tag{7}$$

The Nusselt number of the fully developed flow depends on the sinusoidal channel geometry [24]:

$$Nu = 1.1791\left[1 + 2.7701\left(\frac{a_c'}{b_c'}\right) - 3.1901\left(\frac{a_c'}{b_c'}\right)^2 + 1.9975\left(\frac{a_c'}{b_c'}\right)^3 - 0.4966\left(\frac{a_c'}{b_c'}\right)^4\right] \tag{8}$$

where a'_c is the inner channel height and b'_c is the inner channel base.

The Sherwood number is calculated through the Chilton-Colburn analogy:

$$Le^{1/3} = \frac{Sh}{Nu} \tag{9}$$

The Lewis number is assumed constant and equal to 1 and therefore Nu is equal to Sh.

The heat transfer coefficient h_T can be calculated from local Nusselt number in this way:

$$Nu = \frac{h_T D_{eq}}{k_a} \tag{10}$$

where k_a is the thermal conductivity of the wet air. The mass transfer coefficient h_m is obtained from the Sherwood number:

$$Sh = \frac{h_M D_{eq}}{\rho_{DA} D_v} \tag{11}$$

where D_v is the mass diffusivity of vapour in air.

The actual velocity of air in the channel is assumed to be:

$$u = \frac{v_f}{\sigma} \tag{12}$$

where σ is the wheel porosity calculated in this form:

$$\sigma = \frac{A_c}{A_M + A_c} \tag{13}$$

Finally the following correlations are used to calculate respectively: The equivalent diameter of the inner channel [24], the inner channel height and base, the inner channel cross section area, perimeter and the cross section area of the matrix layer:

$$D_{eq} = a_c'\left[1.0542 - 0.4670\frac{a_c'}{b_c'} - 0.1180\left(\frac{a_c'}{b_c'}\right)^2 + 0.1794\left(\frac{a_c'}{b_c'}\right)^3 - 0.0436\left(\frac{a_c'}{b_c'}\right)^4\right] \tag{14}$$

$$a_c' = a_c - 2\frac{s}{2} \tag{15}$$

$$b_c' = b_c - 2\frac{s}{2} \tag{16}$$

$$A_c = \frac{a_c' b_c'}{2} \tag{17}$$

$$P = b_c + 2\sqrt{\left(\frac{b_c}{2}\right)^2 + \left(\frac{a_c}{2}\pi\right)^2}\,\frac{3 + \left(\frac{2b_c}{\pi a_c}\right)^2}{4 + \left(\frac{2b_c}{\pi a_c}\right)^2} \tag{18}$$

$$A_M = P\frac{s}{2} \tag{19}$$

2.3. Boundary and Initial Conditions

The following conditions are set to solve the system of equations discussed above:

Initial conditions:

$$\begin{cases} T_a(0,z) = T_{a,0} \\ T_M(0,z) = T_{M0} \\ X(0,z) = X_0 \\ W(0,z) = W_0 \end{cases} \tag{20}$$

Boundary conditions supply air period:

$$\begin{cases} T_a(t,0) = T_{su,in} \\ X(t,0) = X_{su,in} \end{cases} \tag{21}$$

And during the exhaust air period:

$$\begin{cases} T_a(t,0) = T_{ex,in} \\ X(t,0) = X_{ex,in} \end{cases} \tag{22}$$

The system of *PDE* (Partial Differential Equations) is solved with the Implicit Euler Method. Convergence is achieved when water mass and heat transferred from air during the supply air period are equal to water mass and heat exchanged during the exhaust air period plus a prefixed error.

2.4. Pressure Drop

Pressure drop is calculated through the following equation:

$$\Delta p = \xi_C \frac{1}{2} \rho_{wa}\, u^2 + 4 f \frac{L}{D_{eq}} \frac{1}{2} \rho_{wa}\, u^2 \tag{23}$$

where ξ_c is the loss coefficient which takes into account the contraction and expansion of the air flow at the inlet and outlet of the wheel, assumed equal to 0.2 [25], and f is the Fanning friction factor, which is expressed in the following form [24]:

$$f\,\mathrm{Re} = 9.5687 \left[1 + 0.0772 \frac{a_c'}{b_c'} + 0.8619 \left(\frac{a_c'}{b_c'} \right)^2 - 0.8314 \left(\frac{a_c'}{b_c'} \right)^3 + 0.2907 \left(\frac{a_c'}{b_c'} \right)^4 - 0.0338 \left(\frac{a_c'}{b_c'} \right)^5 \right] \tag{24}$$

In Equation (24), Reynolds number of each air stream is evaluated at average conditions between the channel inlet and outlet.

3. Experimental Methodology

3.1. Experimental Setup Description

A rotary heat exchanger was tested in two different test rigs: In the first one the sensible effectiveness has been evaluated, while in the second one pressured drop has been measured. The two test rigs are described in detail in Sections 3.2 and 3.3.

3.2. Heat Transfer Test Rig

The facility is designed according to ASHRAE standards [26], in order to provide the rotary heat exchanger with two air streams at balanced and controlled flow rates. Supply and exhaust air flows pass through the heat wheel in a counter current arrangement. A schematic representation of the experimental setup is shown at the top of Figure 2.

Supply air is provided at outdoor temperature, while exhaust air temperature is properly controlled through an electric heater. Humidity ratio of both air streams is not controlled and is equal to outside air humidity ratio. Temperature is measured by calibrated thermocouples (type T Copper/Constantan) with ±0.5 °C uncertainty. Sensors are installed across the heat wheel, at the inlet and outlet of each air stream.

Figure 2. Heat transfer and pressure drop test rigs.

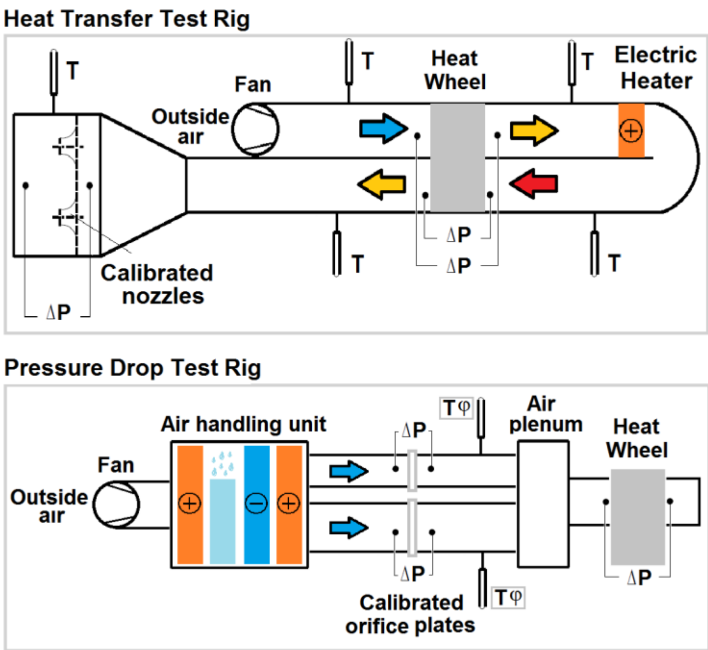

Mass flow rates of the supply and exhaust air streams are equal. Flow rates are set by a variable speed fan and are measured through calibrated nozzles, constructed according to ASHRAE standards [26]. Air flow rate can be adjusted in the range between 1000 and 3000 $m^3 \cdot h^{-1}$. Pressure drop and temperature at calibrated nozzles inlet and outlet are measured through a water U-tube manometer (uncertainty of 1% of reading) and by a calibrated thermocouple (uncertainty of ±0.5 °C) respectively.

Heat wheel revolution speed is controlled through an AC inverter motor in the range between 10 and 20 $rev \cdot min^{-1}$. All calibrated sensors are connected to a specific data logger and samples are collected every 5 s. Air handling unit and ducts are properly insulated with mineral wool panels.

3.3. Pressure Drop Test Rig

A specific facility has been designed to measure the pressure drop across the heat wheel, as shown in Figure 2. In a typical experimental setup used to evaluate heat wheels performance, the measured pressure drop includes the effect of the cross section variation of the ducts which supply the air stream to the device. In fact, the wheel face area has a semi-circular geometry and connecting ducts have a rectangular cross section. Air pressure drop related to this cross section variation does not depend on the heat wheel channels geometry but on the air handling unit and heat exchanger frame design.

In order to exclude the contribution of the aforementioned effect, in this pressure drop test rig a circular duct has been sealed directly to the heat wheel face area. In this way only distributed and local pressure drop at inlet and outlet of the heat wheel channels have been properly measured.

The pressure drop test rig is part of a complex unit that is used to evaluate desiccant wheel performance. Outside air is properly controlled through heating coils, cooling coils and evaporative coolers in order to match the required temperature and humidity.

Air flow rate is set by variable speed fans and is measured across orifice plates installed in two different parallel ducts. Each duct can be excluded in case of low volumetric air flow tests to limit measurement uncertainty. Orifice plates and ducts apparatus are constructed according to DIN EN ISO 5167-2 standards [27]. The maximum air flow rate is 2000 $m^3 \cdot h^{-1}$. A part of the heat wheel face is directly connected to a 20 cm-diameter duct.

Pressure drop across the rotative heat exchanger and across orifice plate is measured by piezoelectric transmitters (uncertainty of ±0.5% of reading ±1 Pa) while temperature is measured by calibrated RTD PT100 1/3 class B (IEC 751) sensors (uncertainty of ±0.2 °C) and relative humidity by capacitive sensors (uncertainty of ±1%).

3.4. Experimental Procedure

Each test is carried out in steady state conditions and in each session at least 100 samples of each physical quantity are logged. Representative values for each working point are obtained as average of the collected data.

At the end of each test the following quantities are calculated:

$$Q_{s,su} = \dot{m}_a \; cp_a \left(T_{su,in} - T_{su,out}\right) \tag{25}$$

$$Q_{s,ex} = \dot{m}_a \; cp_a \left(T_{ex,out} - T_{ex,in}\right) \tag{26}$$

Performance of heat wheel is determined through sensible effectiveness, defined as:

$$\varepsilon_s = \frac{Q_{s,su} + Q_{s,ex}}{2\,\dot{m}_a \; cp_a \; (T_{ex,in} - T_{su,in})} \tag{27}$$

The experimental uncertainty u_{xi} of each monitored variable x_i is:

$$u_{x_i} = \pm\sqrt{u^2_{x_{i,inst}} + (t_{95}\; \sigma_{\bar{x}_i})^2} \tag{28}$$

where $u_{xi,inst}$ is the instrument uncertainty of the generic measured parameter, t_{95} is the Student test multiplier at 95% confidence and $\sigma_{\bar{x}_i}$ is the standard deviation of the mean.

The combined uncertainty of sensible effectiveness $u_{\varepsilon s}$ is calculated as [28]:

$$u_{\varepsilon s} = \sqrt{\sum_i \left(\frac{\partial \varepsilon}{\partial x_i} u_{x_i,inst}\right)^2 + t_{95} \sum_i \left(\frac{\partial \varepsilon}{\partial x_i} \sigma_{\bar{x}_i}\right)^2} \tag{29}$$

Pressure drop has been measured through a specific test, as reported in Section 3.2. Even in this case pressure drop of each test condition has been calculated as the average of the measured values and its uncertainty evaluated through Equation (28).

4. Model Validation

Model results have been compared with experimental data of a commercial heat wheel tested in the two experimental rigs described in Section 3.2 and 3.3. Main data of the tested device are summarized in Table 1.

Table 1. Main data of tested heat wheel.

Parameter	Data
a_c (mm)	2.0
b_c (mm)	3.8
s (mm)	0.055
D (m)	0.6
D_{hub} (m)	0.06
L (m)	0.2
Matrix Material	Aluminium *
Purge Sector	None

* Assumed $\rho_M = 2700$ kg·m^{-3}; $cp_M = 900$ kJ·kg^{-1} °C^{-1}; $k_M = 220$ W·m^{-1}·°C^{-1}.

4.1. Sensible Effectiveness

The heat wheel has been tested in several working conditions, as summarized in Table 2, in particular with different revolution speed and air face velocity and inlet temperature of both air streams.

Table 2. Experimental sensible effectiveness: Test conditions and measured data.

Test	A1	A2	A3	B1	B2	B3	C1	C2	C3	D1	D2	D3	E1	E2	E3	F1	F2	F3
v_f (m s^{-1})	2.09	2.11	2.11	2.87	2.92	2.92	3.76	3.72	3.71	4.44	4.45	4.40	5.21	5.18	5.17	5.75	5.76	5.80
N (rev min^{-1})	10	15	20	10	15	20	10	15	20	10	15	20	10	15	20	10	15	20
$T_{su,in}$ (°C)	25.8	26.2	25.0	24.2	23.8	24.3	22.3	23.3	24.8	22.5	22.6	23.8	20.2	20.1	20.3	21.8	21.3	20.9
$T_{ex,in}$ (°C)	64.5	64.0	62.6	57.3	56.9	55.5	47.4	51.4	53.2	51.8	49.7	49.7	47.3	58.1	59.7	59.6	60.7	59.8
X_{in} (g kg^{-1})	9.1	7.8	8.2	8.2	8.0	8.1	9.8	11.1	9.9	9.3	9.5	9.6	9.8	9.7	9.8	10.5	10.2	10.1
$\varphi_{su,in}$ (%)	44.3	37.2	42.0	44.2	44.0	43.3	59.1	62.6	51.1	55.3	56.3	52.9	67.2	67.0	66.8	65.1	65.3	66.1
$\varphi_{ex,in}$ (%)	6.0	5.3	5.9	7.5	7.5	8.1	14.5	13.4	11.0	11.1	12.5	12.7	14.6	8.5	8.0	8.6	8.0	8.2
ε_s (-)	0.79	0.79	0.79	0.74	0.74	0.74	0.68	0.69	0.69	0.65	0.65	0.65	0.61	0.62	0.62	0.58	0.59	0.60
$Q_{,s}$ (kW)	11.1	10.9	10.9	12.3	12.5	11.8	11.0	12.3	12.5	14.3	13.5	12.8	14.7	20.9	21.8	21.8	23.2	23.1

In Figure 3 the comparison between experimental data and simulation results is reported and good agreement is achieved. It is shown that the maximum relative error between model and data is always lower than 5% and, in all conditions except for tests A1, A2 and A3 ($v_f \approx 2.1$ m·s^{-1}), calculated sensible effectiveness is within the experimental uncertainty. Therefore it is possible to state that the model is able to well predict the heat transfer of the heat wheel.

Figure 3. Sensible effectiveness: Experimental data and simulation results. Refer to Tables 1 and 2 for heat wheel data and test conditions.

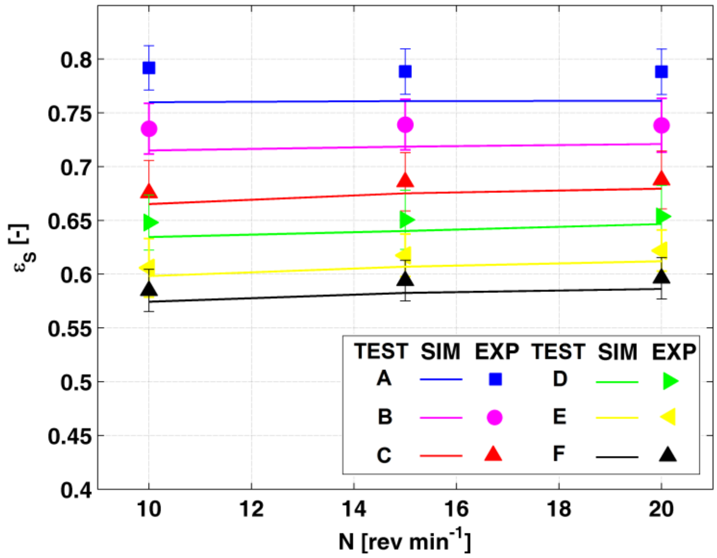

4.2. Pressure Drop

Pressure drop of the heat wheel has been evaluated at constant temperature and humidity ratio (T_a = 25.0 °C and X_a = 8.2 g/kg). Figure 4 shows experimental and numerical values of pressure drop for different face velocities. Good agreement between data and simulations is achieved: the maximum relative error is lower than 15% and around 5% in most cases. The quasi-linear behaviour put in evidence that local pressure drop is negligible compared to distributed pressure drop in the channel. Based on data reported in Figure 4, it is possible to state that local pressure drop calculated in Equation (23) is slightly underestimated, while the distributed pressure drop calculated through Equation (24) is slightly overestimated.

Figure 4. Pressure drop: experimental data and simulation results at T_a = 25.0 °C, X_a = 8.2 g kg^{-1} and φ_a = 42%. Refer to Table 1 for heat wheel data.

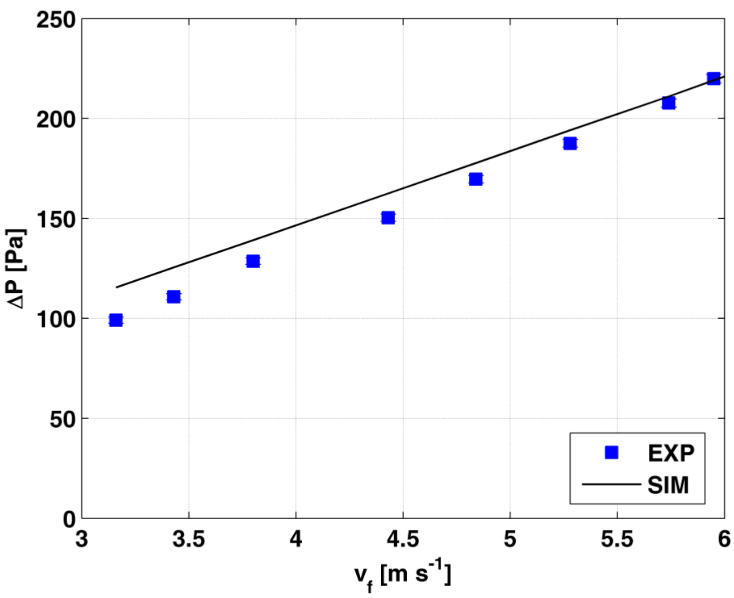

5. Heat Wheel Optimization

5.1. Preliminary Analysis of Performance

In this section the effect of boundary conditions and design parameters on heat wheel sensible effectiveness is evaluated. These effects are investigated for a rotary heat exchanger crossed by balanced supply and exhaust air flows. In all simulations face air velocity is an input and results are reported at constant face area. It is assumed the heat wheel is made of aluminium, whose properties are reported in Table 1. Although the model is able to predict latent heat recovery due to water condensation on channel walls, in this work only sensible effectiveness is analysed and therefore appropriate boundary conditions have been selected.

In Figure 5 it is shown the effect of revolution speed, inlet temperature and face velocity on component effectiveness. It is possible to state that if inlet temperature of air streams varies within the range of HVAC applications, the rotary heat exchanger performance does not change significantly. On the other side, effects due to revolution speed and face velocity variation are important and they can be explained in the following way:

- If the heat wheel rotates too slowly, the matrix material average temperature becomes close to the air stream and, therefore, heat transfer decreases due to limited temperature difference. On the other side, if the wheel rotates too fast, the effect of carryover, *i.e.*, the cross contamination between the two streams due to the amount of air trapped in the wheel channel, becomes relevant. Therefore an optimal revolution speed exists: It is typically around 10–20 rev·min^{-1}, depending on air flow rates and heat exchanger geometry.
- If the face air velocity v_f of both streams increases (and consequently the velocity in the channel u), the sensible effectiveness decreases because air heat capacity rate is bigger at constant heat transfer area.

All the aforementioned considerations are in agreement with previous research works, such as [13,17,18].

Figure 5. Effect of revolution speed, inlet temperature and face velocity on sensible effectiveness ($a_c = b_c = 2$ mm, $s = 0.06$ mm, $L = 0.2$ m, $X_{a,in} = 3.0$ g/kg).

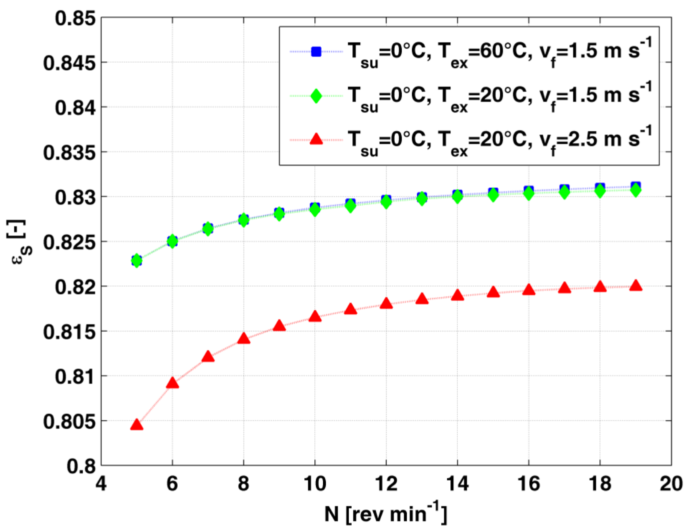

In Figure 6a parametric analysis of sensible effectiveness and pressure drop as a function of the variation of several boundary conditions and heat wheel design parameters is shown. Each parameter is varied within ±20% of a reference condition. The following considerations are put in evidence:

- The higher the wheel length *L*, the higher the effectiveness and pressure drop. In fact the heat transfer area increases proportionally to the wheel length.
- The higher the channel thickness *s*, the lower the effectiveness. In this working condition, the trend can be explained considering that the increase in *s* leads to an increase in the wheel mass and thermal capacity. Therefore during each rotation the temperature variation of the wheel matrix decreases and, as a consequence, also the pinch-point between the matrix and each outlet air stream, reducing the heat transfer. In addition the wheel porosity decreases and, therefore, the air velocity *u* in the channel increases, leading to the previously described effects and to a slight increase in pressure drop.
- Regarding the channel geometry, the increase in either a_c or b_c or both a_c and b_c with constant thickness leads to a bigger channel hydraulic diameter and, therefore, to a lower heat transfer area and heat transfer coefficient. These effects lead to a sensible effectiveness reduction. Note that this variation is less relevant if only the channel height a_c is increased, because in this case, according to Equation (8), even the Nusselt number increases, with positive results on the heat transfer coefficient. Similarly the lower the heat transfer area, the lower pressure drop.
- The effects of the variation of the face velocity v_f and of the revolution speed *N* on sensible effectiveness are in agreement with results reported in Figure 5. In addition, there is an almost linear relationship between pressure drop and air velocity, showing that distributed pressure drop is prevailing on local one.

Figure 6. Parametric analysis of sensible effectiveness and pressure drop. (Reference conditions: $a_c = 2$ mm, $b_c = 2$ mm, $s = 0.06$ mm, $L = 0.2$ m, $v_f = 1.5$ m·s^{-1}, $N = 10$ rev·min^{-1} $T_{su,in} = 10$ °C, $T_{ex,in} = 30$ °C, $X_{su,in} = 3.7$ g·kg^{-1}, $X_{ex,in} = 7.7$ g·kg^{-1}, $\varphi_{su,in} = 50\%$ and $\varphi_{ex,in} = 30\%$).

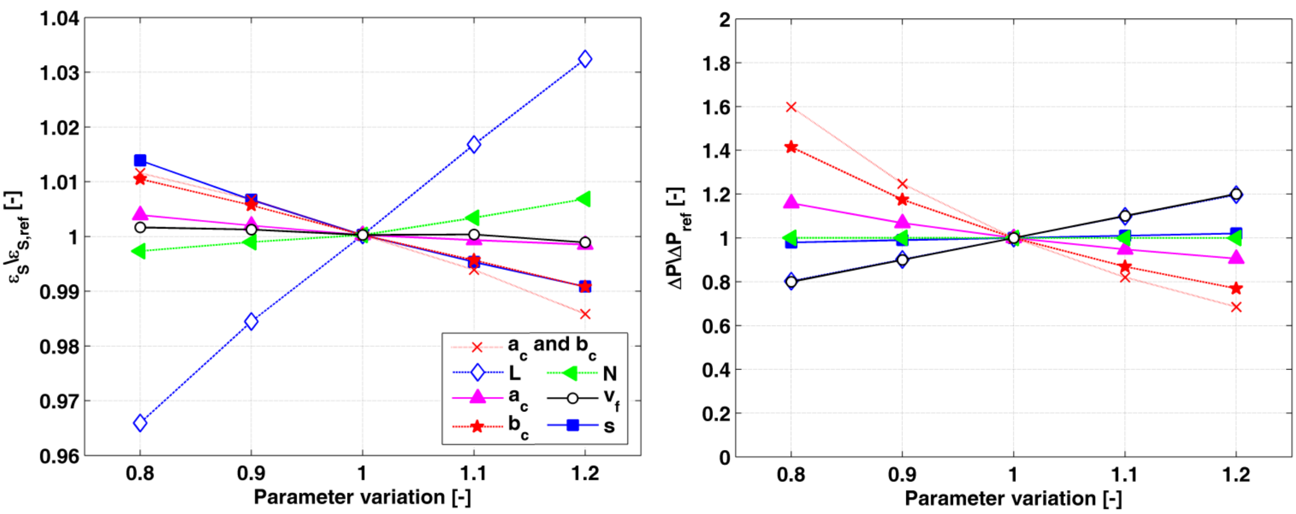

5.2. Optimization Results

5.2.1. Preliminary Simulations

In this section the heat wheel design is optimized in order to maximize effectiveness and minimize pressure drop, which is directly related to ventilation power consumption. The power required to rotate the device (around 30 W for a 60 cm-diameter wheel) is not considered. According to the preliminary investigation reported in Section 5.1, the analysis is performed at fixed inlet temperature and humidity ratio of both air streams. Note that inlet air conditions are not strictly representative of a specific site but they have been fixed in order to avoid water condensation on the wheel channel. Many parameters affecting heat exchanger sensible effectiveness and pressure drop have been varied, namely: Channel height, base and thickness, revolution speed, wheel length and face air velocity.

Each of the aforementioned parameters has been varied in the range reported in Table 3. According to Equations (8) and (9) typical values of *Nu* and *Sh* are in the range between 2.1 and 2.6 while *Re* varies between 100 and 550 ($v_f = 2.5$ m s^{-1}).

Table 3. Minimum and maximum value of each parameter adopted in the simulations.

Parameter	Min	Max
N (rev·min^{-1})	5	20
a_c (mm)	1	6
b_c (mm)	1	6
s (mm)	0.05	0.12
L (m)	0.05	0.4
v_f (m·s^{-1})	1.5	3.5

Results are reported in Figure 7: It is possible to state that for each air face velocity there is a clear boundary along which sensible effectiveness is maximised as a function of pressure drop (for example at $v_f = 1.5$ m·s^{-1} and $\Delta P = 50$ Pa, the maximum achievable effectiveness is $\varepsilon_s = 0.8$).

Figure 7. Sensible effectiveness against pressure drop for different heat wheel geometry and boundary conditions (see Table 3, $T_{su,in}$ = 10 °C, $T_{ex,in}$ = 30 °C, $X_{su,in}$ = 3.7 g·kg^{-1}, $X_{ex,in}$ = 3.7 g·kg^{-1}, $\varphi_{su,in}$ = 50% and $\varphi_{ex,in}$ = 30%).

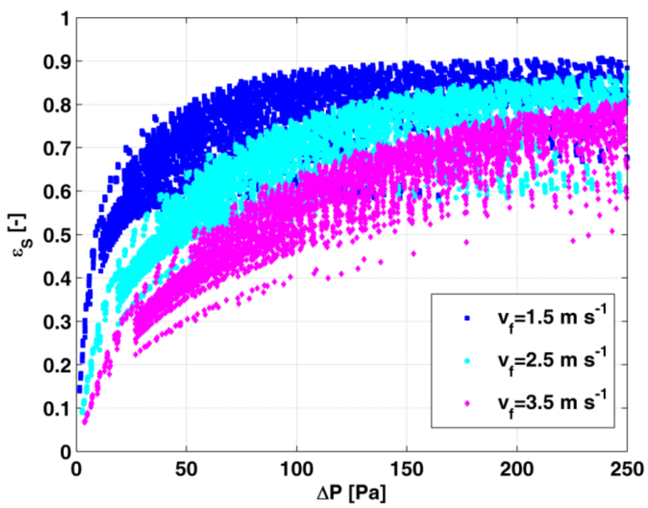

It is of primary interest to identify the values that design parameters should assume in order to match the Pareto front. It is outlined that points on Pareto front are marked out by small channel thickness and are almost independent of revolution speed, that is generally around 8–12 rev·min^{-1}. In order to evaluate properly the effect of other parameters, a detailed analysis has been performed in case of v_f = 2.5 m·s^{-1}, which represents a common operating condition in air handling units.

5.2.2. Performance at Constant Heat Wheel Length L = 0.2 m

It is put in evidence that the length of most commercial rotary heat exchangers is usually equal to 0.2 m [9], according to air handling units' manufacturer requirements. Therefore a preliminary investigation deals with such a configuration: In Figure 8 the optimal heat wheel arrangements with L = 0.2 m are shown. Based on the preliminary analysis of Section 5.2.1, in all cases the best channel thickness is s = 0.05 mm, that is the minimum value adopted in the simulations. A thinner channel is not considered because of its lack of mechanical resistance.

Figure 8. Optimal heat wheel configurations at L = 0.2 m and at v_f = 2.5 m·s^{-1} for different channel height and base ($T_{su,in}$ = 10 °C, $T_{ex,in}$=30 °C, $X_{su,in}$ = 3.7 g·kg^{-1}, $X_{ex,in}$ = 7.7 g·kg^{-1}, $\varphi_{su,in}$ = 50%, $\varphi_{ex,in}$ = 30%, s = 0.05 mm and N = 10 rev·min^{-1}).

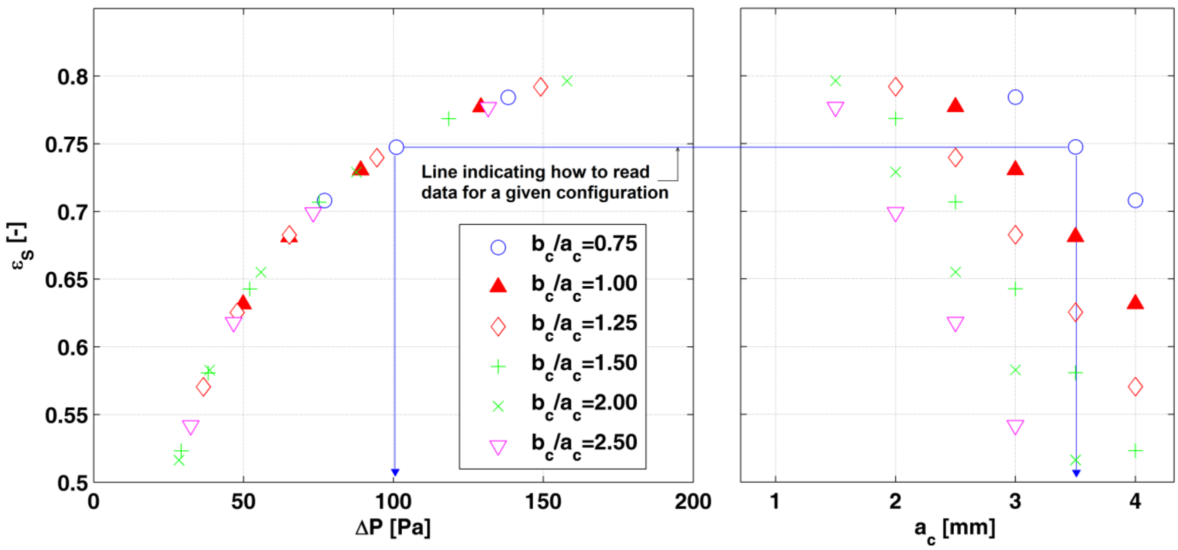

It is known that the reduction of the channel aspect ratio b_c/a_c or the channel height leads to an increase in effectiveness and pressure drop. Analyzing data reported in Figure 8, it is shown that all results almost fit a curve representing, for a given pressure drop, the optimal achievable effectiveness with L = 0.2 m. Each point of the curve can be attained through several heat wheel configurations. For example, the condition ε_s = 0.73 and ΔP = 88 Pa can be achieved either with a_c = 2 mm and b_c = 4 mm or a_c = 3 mm and b_c = 3 mm. Similarly, it is possible to state that the curve in Figure 8 can be fitted by varying the channel base and height at constant aspect ratio. For instance if b_c/a_c = 2 and a_c is varied between 1.5 and 3.5 mm, the sensible effectiveness ε_s is within the range 0.8 (ΔP = 158) to 0.51 (ΔP = 30).

In conclusion if L = 0.2 m, the best performance can be obtained through many heat wheels configurations. All devices arrangements are characterized by a thin channel thickness (s = 0.05 mm), by a revolution speed N around 10 rev min^{-1} and by different values of channel size. Therefore in the analysis reported in the next section, only the aspect ratio $b_c/a_c = 2$ is considered in order to limit the amount of cases to be analyzed.

5.2.3. Performance at Constant Channel Aspect Ratio $b_c/a_c = 2$

Based on the considerations reported in Section 5.2.2, heat wheel performance at constant aspect ratio and different wheel length are evaluated. In Figure 9 sensible effectiveness *versus* pressure drop at $b_c/a_c = 2$ and for different wheel length and channel dimensions is shown. In this case, quite obviously, the higher the length, the higher the effectiveness and the pressure drop. At low effectiveness ($\varepsilon_s < 0.65$), the same results can be obtained with different wheel arrangements having almost the same pressure drop. For example comparable results are achieved if $a_c = 2.5$ mm and $L = 0.15$ m or if $a_c = 3.0$ mm and $L = 0.2$ m.

Figure 9. Optimal wheel configurations at constant channel aspect ratio $b_c/a_c=2$ and at $v_f = 2.5$ m·s^{-1} for different length ($T_{su,in} = 10$ °C, $T_{ex,in} = 30$ °C, $X_{su,in} = 3.7$ g·kg^{-1}, $X_{ex,in} = 7.7$ g kg^{-1}, $\varphi_{su,in} = 50\%$, $\varphi_{ex,in} = 30\%$, $s = 0.05$ mm and $N = 10$ rev·min^{-1}).

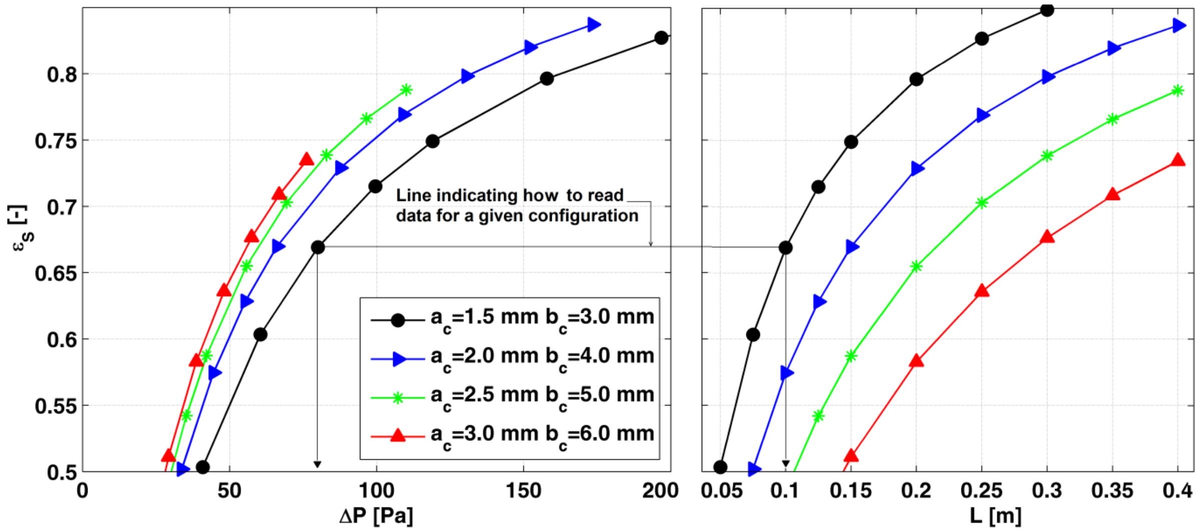

Instead, if higher effectiveness is required, both channel dimensions and wheel length should be increased. For instance, sensible effectiveness $\varepsilon_s = 0.735$ can be reached with $a_c = 3.0$ mm and $L = 0.4$ m or with $a_c = 1.5$ mm and $L = 0.12$ m: In the second case pressure drop is 45% higher than the first one.

5.2.4. Performance Optimization

Comparing Figures 8 and 9, it is possible to state that it is better to increase sensible effectiveness through the increase in wheel length instead of the reduction in channel hydraulic diameter. Anyway, if $\varepsilon_s < 0.65$ optimal configurations minimizing pressure drop for a given effectiveness can be reached also with small wheel length ($L < 0.2$ m) and through appropriate channel dimensions. Instead, if $\varepsilon_s > 0.65$, the increase in wheel length is essential to attain the best configuration. According to Figures 8 and 9, it is possible to state that:

- When L = 0.2, the heat wheel is almost optimized if b_c > 3.8–4.0 mm and b_c/a_c > 1. In other arrangements, for a given effectiveness, pressure drop is higher than the value attained with the best configuration.
- If there are no restrictions on wheel length, a large hydraulic diameter should be selected (for example with b_c = 6.0 mm and b_c/a_c = 2) and the increase in effectiveness should be obtained through the increase in wheel length. When wheel length cannot be further increased (for example L = 0.4), the increase in effectiveness should be achieved through a reduction in b_c and b_c/a_c. In this way pressure drop is minimized for a given sensible effectiveness.

Note that a similar analysis has been performed also with v_f = 1.5 m·s^{-1} and v_f = 3.5 m·s^{-1}, confirming the aforementioned results and considerations. Finally, in Figure 10 effectiveness, pressure drop and amount of matrix material are shown for different L and a_c. The matrix material per unit of face area M_M is calculated as follows:

$$M_M = (1 - \sigma)\, L\, \rho_M \tag{30}$$

Figure 10. Sensible effectiveness, pressure drop and amount of matrix material for different L and a_c (b_c/a_c = 2, $T_{su,in}$ = 10 °C, $T_{ex,in}$ = 30 °C, $X_{su,in}$ = 3.7 g·kg^{-1}, $X_{ex,in}$ = 7.7 g·kg^{-1}, $\varphi_{su,in}$ = 50%, $\varphi_{ex,in}$ = 30%, s = 0.05 mm, N = 10 rev·min^{-1} and v_f = 2.5 m·s^{-1}).

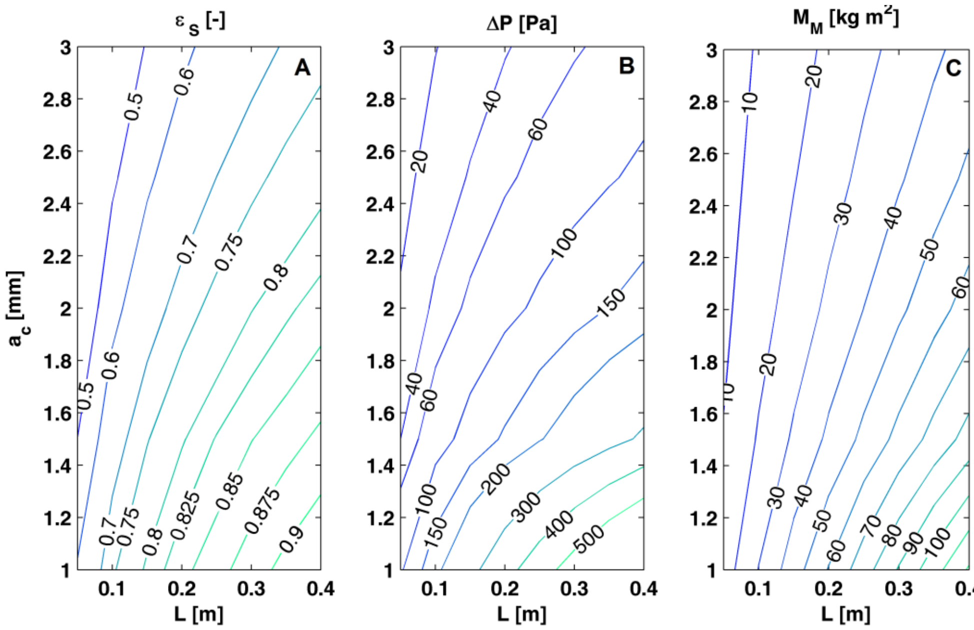

Comparing contour maps A and B of Figure 10, it is put in evidence that for a given effectiveness, it is better to increase L rather than reduce a_c due to the lower pressure drop. Instead, analysing contour maps A and C of Figure 10, it is shown that the slope of the effectiveness and the matrix material per unit of face area are very similar: Therefore heat wheels optimized through the increase of L require almost the same amount of material of wheels whose effectiveness is increased through the reduction of the channel hydraulic diameter.

6. Conclusions

In this paper a detailed optimization of heat wheels design parameters is performed in order to maximize sensible effectiveness and to minimize pressure drop. The analysis is carried out through a validated one dimensional lumped parameters heat wheel model and through appropriate correlations to estimate pressure drop. The device optimization is performed through the variation of main design parameters and operating conditions: Wheel length, channel base, height and thickness, air face velocity and revolution speed. As a result of the optimization process, the following considerations should be underlined:

- The best configurations are characterized by a small channel thickness (for example s = 0.05 mm).
- Revolution speed barely affects wheel performance and, therefore, N should be within 10–15 rev·min^{-1}.
- Heat wheels with large channel hydraulic diameters should be preferred (for example b_c = 5.0–6.0 mm and b_c/a_c = 1.5–2) and the increase in sensible effectiveness should be reached through the increase in the wheel length.
- If the wheel length is equal to 0.2 m due to air handling units manufacturer restrictions, the component is almost optimized if b_c > 3.8–4.0 mm and b_c/a_c > 1.
- Heat wheels optimized through the increase in L do not require more matrix material than wheels optimized through the reduction of the channel hydraulic diameter.

Acknowledgments

Funding for this work from Italian Cassa Conguaglio Sistema Elettrico under agreement No. 6562 is acknowledged (project STAR-Sidera Trigenerazione Alto Rendimento).

Author Contributions

All the authors have previous experience on heat wheels that have been shared in order to reach the results discussed in the paper. In particular Stefano De Antonellis, Manuel Intini and Cesare Maria Joppolo contributed to the development of the heat wheel model and to the optimization analysis while Calogero Leone contributed to the technical development of the experimental set-up. All the authors equally contributed to the preparation and to the critical revision of the paper.

Nomenclature

a_c	channel height (m)
a'_c	inner channel height (m)
A_c	channel cross section area (m^2)
A_M	matrix layer cross section area (m^2)
b_c	channel base (m)
b'_c	inner channel base (m)
c_p	isobaric specific heat (J·kg^{-1}·K^{-1})
D	external wheel diameter (m)

D_{hub}	wheel hub diameter (m)
D_v	diffusivity of water vapour in air ($m^2 \cdot s^{-1}$)
D_{eq}	hydraulic channel diameter (m)
EXP	experiment
f	Fanning friction factor (-)
f_M	matrix mass per unit of length ($kg \cdot m^{-1}$)
h_m	mass transfer coefficient ($kg \cdot m^{-2} \cdot s^{-1}$)
h_T	heat transfer coefficient ($W \cdot m^{-2} \cdot K^{-1}$)
k	thermal conductivity ($W \cdot m^{-1} \cdot K^{-1}$)
L	wheel length (m)
Le	Lewis number (-)
$\dot{m}$	mass flow of dry air ($kg \cdot s^{-1}$)
M	mass per unit of face area ($kg \cdot m^{-2}$)
N	wheel rotational speed ($rev \cdot min^{-1}$)
p	pressure (Pa)
P	channel perimeter (m)
Q_s	heat transfer rate (W)
Re	Reynolds number (-)
s	channel thickness (m)
Sh	Sherwood number (-)
SIM	simulation
t	time (s)
T	temperature (°C)
u	air velocity in the channel ($m \cdot s^{-1}$)
v_f	face air velocity ($m \cdot s^{-1}$)
W	water content ($kg \cdot kg^{-1}$)
X	air humidity ratio ($kg \cdot kg^{-1}$)
x_i	monitored physical variable (-)
z	axial direction (m)
Greek letters	
ΔP	pressure drop (Pa)
ε_s	sensible effectiveness (-)
λ	latent heat of vaporization ($kJ \cdot kg^{-1}$)
ξ_C	local pressure drop coefficient (-)
ρ	density ($kg\ m^{-3}$)
σ	wheel porosity (-)
φ	relative humidity (-)
Subscripts	
0	initial condition
a	air
da	dry air
dew	air dew point

ex	exhaust air
in	inlet
inst	instrumental
M	channel material
out	outlet
sat	saturated vapour
su	supply air
tot	total
v	water vapour
w	liquid water
W	channel wall
wa	wet air

Conflicts of Interest

The authors declare no conflict of interest.

References

1. Mardiana, A.; Riffat, S.B. Review on physical and performance parameters of heat recovery systems for building applications. *Renew. Sustain. Energy Rev.* **2013**, *28*, 174–190.
2. Valancius, R.; Jurelionis, A.; Dorosevas, V. Method for cost-benefit analysis of improved indoor climate conditions and reduced energy consumption in office buildings. *Energies* **2013**, *6*, 4591–4606.
3. Airaksinen, M. Energy use in day care centers and schools. *Energies* **2011**, *4*, 998–1009.
4. Tommerup, H.; Svendsen, S. Energy savings in Danish residential building stock. *Energy Build.* **2006**, *38*, 618–626.
5. Rasouli, M.; Simonson, C.J.; Besant, R.W. Applicability and optimum control strategy of energy recovery ventilators in different climatic conditions. *Energy Build.* **2010**, *42*, 1376–1385.
6. Leone, C.; Liberati, P. Designing the comfort and the energy savings through the heat recovery use. In Proceedings of the AICARR National Conference 2014, Padua, Italy, 5 June 2014.
7. Dall'O', G.; Belli, V.; Brolis, M.; Mozzi, I. Fasano, M. Nearly Zero-Energy Buildings of the Lombardy Region (Italy), a Case Study of High-Energy Performance Buildings. *Energies* **2013**, *6*, 3506–3527.
8. Airaksinen, M.; Matilainen, P. A Carbon Footprint of an Office Building. *Energies* **2011**, *4*, 1197–1210.
9. Eurovent Certified Performance. Available online: http://www.eurovent-certification.com (accessed on 1 September 2014).
10. Nóbrega, C.E.L.; Brum, N.C.L. Modeling and simulation of heat and enthalpy recovery wheels. *Energy* **2009**, *34*, 2063–2068.
11. Wu, Z.; Melnik, R.V.; Borup, F. Model-based analysis and simulation of regenerative heat wheel. *Energy Build.* **2006**, *38*, 502–514.

12. Simonson, C.J.; Besant, R.W. Energy wheel effectiveness: Part I-development of dimensionless groups. *Int. J. Heat Mass Transf.* **1999**, *42*, 2161–2170.
13. Zhang, L.Z.; Niu, J.L. Performance comparisons of desiccant wheels for air dehumidification and enthalpy recovery. *Appl. Therm. Eng.* **2002**, *22*, 1347–1367.
14. Simonson, C.J.; Besant, R.W. Energy wheel effectiveness: Part II–correlations. *Int. J. Heat Mass Transf.* **1999**, *42*, 2171–2185.
15. Sphaier, L.A.; Worek, W.M. Parametric analysis of heat and mass transfer regenerators using a generalized effectiveness-NTU method. *Int. J. Heat Mass Transf.* **1999**, *52*, 2265–2272.
16. De Antonellis, S.; Intini, M.; Joppolo, C.M.; Pedranzini, F. Experimental analysis and practical effectiveness correlations of enthalpy wheels. *Energy Build.* **2014**, *84*, 316–323.
17. Jeong, J.W.; Mumma, S.A. Practical thermal performance correlations for molecular sieve and silica gel loaded enthalpy wheels. *Appl. Therm. Eng.* **2005**, *25*, 719–740.
18. Rabah, A.A.; Fekete, A.; Kabelac, S. Experimental Investigation on a Rotary Regenerator Operating at Low Temperatures. *J. Therm. Sci. Eng. Appl.* **2009**, *1*, 041004:1–041004:9.
19. Tu, R.; Liu, X.H.; Jiang, Y. Performance comparison between enthalpy recovery wheels and dehumidification wheels. *Int. J. Refrig.* **2013**, *36*, 2308–2322.
20. Enteria, N.; Yoshino, H.; Satake, A.; Mochida, A.; Takaki, R.; Yoshie, R.; Mitamura, T.; Baba, S. Experimental heat and mass transfer of the separated and coupled rotating desiccant wheel and heat wheel. *Exp. Therm. Fluid Sci.* **2010**, *34*, 603–615.
21. Mioralli, P.C.; Ganzarolli, M.M. Thermal analysis of a rotary regenerator with fixed pressure drop or fixed pumping power. *Appl. Therm. Eng.* **2013**, *52*, 187–197.
22. Swanepoel, D.C.; Kröger, D.G. Rotary regenerator design theory and optimisation. *Res. Dev. J. Afr. Inst. Mech. Eng.* **1996**, *12*, 90–97.
23. Yilmaz, A.; Büyükalaca, O.; Yilmaz, T. Optimum shape and dimensions of ducts for convective heat transfer in laminar flow at constant wall temperature. *Int. J. Heat Mass Transf.* **2000**, *43*, 767–775.
24. Kakac, S.; Shah, R.K.; Aung, W. *Handbook of Single Phase Convective Heat Transfer*; John Wiley & Sons: New York, NY, USA, 1987.
25. Niu, J.L.; Zhang, L.Z. Heat transfer and friction coefficient in corrugated ducts confined by sinusoidal and arc curves. *Int. J. Heat Mass Transf.* **2002**, *45*, 571–578.
26. *Method of Testing Air-to-Air Heat/Energy Exchangers*; ANSI/ASHRARE 84-2008; American Society of Heating, Refrigerating and Air Conditioning Engineers (ASHRAE): Atlanta, GA, USA, 2008.
27. *Measurement of Fluid Flow by Means of Pressure Differential Devices Inserted in Circular Cross-Section Conduits Running Full-Part 2: Orifice Plates*; DIN EN ISO 5167–2 Standards (ISO 5167–2:2003); International Organization for Standardization: Geneva, Switzerland, 2003.
28. Moffat, R.J. Describing the uncertainties in experimental results. *Exp. Therm. Fluid Sci.* **1988**, *1*, 3–10.